ECS Transactions, 68 (1) 3395-3406 (2015)
10.1149/06801.3395ecst ©The Electrochemical Society

Steam and Co-electrolysis Sensitivity Analysis on Ni-YSZ Supported Cells

G. Rinaldi, S. Diethelm, J. Van herle

FuelMAT Group, Institute of Mechanical Engineering (IGM), Faculty of Engineering (STI), École Polytechnique Fédérale de Lausanne (EPFL), 1015 Lausanne, Switzerland

The present paper investigates the variation in performances in steam electrolysis and co-electrolysis of steam/CO_2 on SOEC single cells. In electrolysis mode, a sensitivity analysis was performed looking in particular at the effects of temperature (750°C and 800°C) and inlet gas flows (from 100 to 200 Nml/min) on the performances. I-V characterization and EIS measurements at different current densities were carried out for each sequence. As expected, the increase of temperature has a positive impact on the performances, while the change of feed flow slightly affects them. In co-electrolysis mode CO_2 and H_2O content was varied, keeping constant the total molar flow and the hydrogen fraction. Resulting plots demonstrate different ongoing processes favored at high current densities and high inlet CO_2 molar fraction. In particular, the reverse water-gas-shift reaction plays an important role on the overall balance of the gas species, and it directly depends on temperature and inlet flow composition.

Introduction

High temperature steam and CO_2 co-electrolysis offers an alternative way to store electrical energy into chemical fuels that are characterized by high energy density. Using electricity from carbon-free sources (nuclear or renewable), this process can convert steam and CO_2 to syngas (CO and H_2), which can be transformed to synthetic natural gas or to methanol or other liquid fuels through technologically mature systems (methanol synthesis and F-T synthesis) (1). Oxygen or enriched air can be obtained as added value (2). Compared to electrolysis of H_2O (Eq. [1]) or CO_2 (Eq. [2]), co-electrolysis is more complex because of the reversible water gas-shift-reaction (RWGS, Eq. [3]), which at high temperatures is shifted to the production of CO and H_2O and the consumption of CO_2 and H_2.

$$H_2O_{(g)} + 2e^- \rightarrow H_{2(g)} + O^{2-} \quad [1]$$

$$CO_{2(g)} + 2e^- \rightarrow CO_{(g)} + O^{2-} \quad [2]$$

$$CO_{2(g)} + H_{2(g)} \rightarrow CO_{(g)} + H_2O_{(g)} \quad [3]$$

Since CO_2 reduction can occur through reactions 2 and 3, the CO production pathway is not yet fully understood. According to the study presented by S. Kim et al (3), CO_2 reduction is dominated by the RWGS reaction, which is predominant at temperatures higher than 800°C and at high CO_2 concentrations. Moreover, results showed that steam

is a primary reactant in co-electrolysis, attributed to its lower activation energy and larger diffusion coefficient in comparison with that of CO_2.

High temperature electrolysis has also a thermodynamic advantage, since a higher fraction of heat and corresponding smaller fraction of electricity is needed for the dissociation (4). Depending on the specific conditions of operation, heat can be provided by reaction losses (Joule heat) or by an external source (industry waste heat or concentrated solar). High temperatures also imply faster reaction kinetics, which reduces the requirement of additional catalyst materials.

In this study, electrochemical responses of reactions taking place in the fuel electrode of intermediate temperature solid oxide cells for steam electrolysis and co-electrolysis are experimentally examined. Key operating parameters including temperature, current density, inlet feed flow and molar ratio of CO_2 to steam were varied systematically, all of which impact both kinetics and species transport. Data acquired are compared and analyzed through I-V curves, Nyquist plots and the derivative of the real part of impedance with respect to the derivative of frequency logarithmic plots.

Experiment Description

Experiment Setup

The cell type under investigation is a circular (Φ 60mm) Ni-YSZ supported cell (240 ± 20 µm) produced by SOLIDpower (5) ("ASC-700" type cell (6)). The thin film electrolyte is constituted by YSZ (8 ± 2 µm) and the oxygen electrode by LSCF-GDC (50 ± 10 µm). The active area corresponds to 12.56 cm^2 (2 cm of radius).

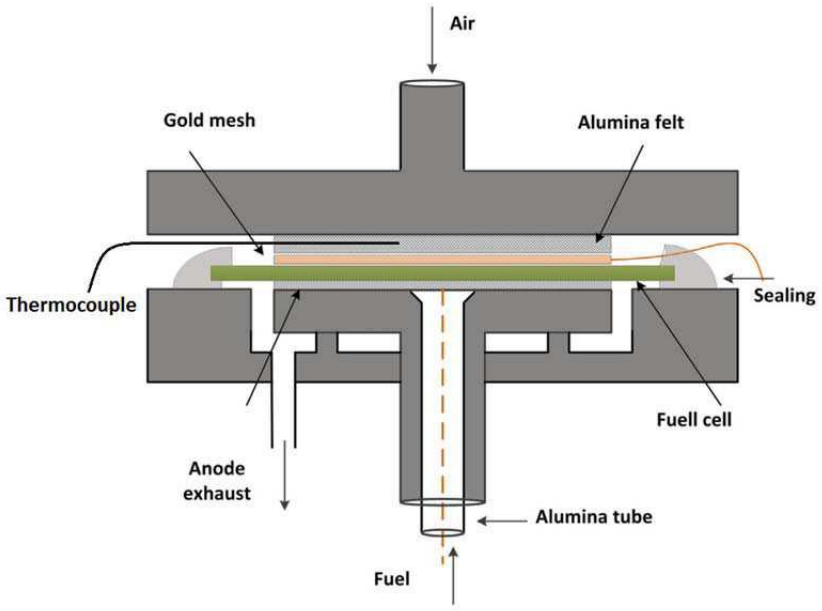

Figure 1. Schematic diagram of experiment setup (7).

Figure 1 represents the scheme of the metallic setup developed and used to support the cell in the furnace. The feed flow is sent to the cell through a ceramic tube inserted in

the metal holder tube. The gas diffuses through a nickel grid that guarantees the current collection, and the exhaust is collected in an outlet tube heated with an electrical resistance in order to prevent condensation of steam. On the oxygen side, inlet air is injected as sweep gas and the outlet flow spreads directly in the furnace. A gold mesh is applied as current collector and an alumina (Al_2O_3) felt is used to distribute the air flow. A K-type thermocouple is positioned for temperature measurement while glass sealing avoids the gas interaction between the two sides. Four springs mounted at each corner of the setup guarantee the selected load on the cell surface. Two different experiments were conducted varying the total load, which corresponded to 0.6 kg/cm^2 for the first one and to 0.4 kg/cm^2 for the second one.

The test station has the capability of controlling the inlet gas concentration of H_2 and CO_2 by mixing to the desired partial pressures using a set of mass flow controllers (Red-y Vögtlin Instruments AG). Deionized water was fed using a peristaltic pump (Ismatec, Switzerland) into an evaporator integrated in the setup (Fiaxell, (8)), where H_2O evaporates and mixes with the other inlet gas species using the heat provided by the furnace.

The cell was heated from room temperature to 750°C at a rate of 100°C/h in four steps to cure the glass seal. During the heating phase, the fuel electrode was fed with 50 Nml/min of Ar and the oxygen electrode with 100 Nml/min of air. After this process, the fuel electrode was reduced with a flow of 150 Nml/min in two steps, first providing a concentration of 80% Ar - 20% H_2 and then 30% Ar - 70% H_2. Under these conditions, the cell was operated at 0.4 A/cm^2 for 24 h until cell voltage stabilized (to 0.881V in this case). The cell was then brought back to OCV and the inlet gas composition shifted to 10% H_2 and 90% H_2O (reference condition for steam electrolysis). The OCV value measured at this stage was 0.853V. During the experiments the cells were fed with different H_2O/CO_2 mixtures, while always keeping 10% H_2 of the inlet molar flow in order to avoid re-oxidation of the Ni-YSZ support.

Electrochemical Impedance Measurements

Electrochemical measurements (EIS and I-V) were performed with an IM6 electrochemical workstation coupled with a booster PP241 (Zahner Elektrik, Germany) using a two-electrode configuration with four wires. I-V curves were done in potentiostatic control mode from OCV to 1.5 V using 5 mV/s as scanning speed (current range of 0 – -15A in order to prevent cell damage).EIS measurements were performed in galvanostatic control mode with 200mA of perturbation in the frequency range from 50 kHz to 0.05 Hz, both at open circuit voltage (OCV) and under current bias. Data smoothing was made using the Zahner software.

All the data acquired were modified in order to remove the parasitic inductance from spectra at high frequencies. This correction is important to properly estimate ohmic (and polarization) resistances. In order to reduce the effect, first the equivalent inductance is calculated in the “vertical” imaginary part of the impedance region at high frequencies, as explained by B. Liu et al. (9). With this value, the initial inductive impedance can be obtained and subtracted to the measured imaginary part of the impedance response at each frequency.

Two different plot typologies are reported in this analysis: the first one, Nyquist plot, relates real (Z') and negative imaginary part of impedance (-Z''). The second typology has a similar appearance as the Bode plot (-Z'' vs frequency) and is obtained from the derivative of the real part of impedance with respect to the derivative of the frequency logarithm (10), (11), (12). This method guarantees a better resolved representation of the different peaks generated by processes occurring at different frequencies.

Results and Discussion

Steam Electrolysis

In this paragraph, steam electrolysis sensitivity analysis measurements are analyzed. I-V curves, Nyquist and real part of impedance derivative plots are reported at two different temperatures (750°C and 800°C) varying four values of current density (0, -0.4, -0.8 and -1.2 A/cm^2). Inlet feed flow was imposed at 150 Nml/min at the fuel electrode (90% H_2O - 10% H_2), and 500 Nml/min of air at the oxygen electrode. In this case, the load applied on the cell was 0.6 kg/cm^2.

As it is evident from the I-V plot (Figure 2-A), temperature increase facilitates reaction kinetics and lowers the internal resistance of the cell, favoring the overall performances. OCV varied from 0.853 at 750°C to 0.830 at 800°C. Table 1 displays the change in ohmic and polarization resistances obtained from the Nyquist plots (Figure 2-B and 2-C), which both benefit of the temperature rise (in particular ohmic resistance). With the variation of current density, polarization resistance drops while ohmic resistance remains almost unaffected. At -1.2 A/cm^2 the polarization resistance increases strongly since a conversion limitation starts to occur at this current density (76% of steam conversion calculated through Faraday's law [4]). In addition, temperature difference has a strong impact on the polarization resistances.

$$\text{Steam conversion} = \frac{\frac{I}{2F}}{\dot{N}_{H_2O_{inlet}}} \qquad [4]$$

TABLE 1. Steam electrolysis temperature variation

Current applied (A/cm^2 - A)	$R_{ohm\text{-}750°C}$ (ohm cm^2)	$R_{pol\text{-}750°C}$ (ohm cm^2)	$R_{ohm\text{-}800°C}$ (ohm cm^2)	$R_{pol\text{-}800°C}$ (ohm cm^2)
0	0.18	0.38	0.12	0.39
-0.4 / -5	0.18	0.19	0.13	0.15
-0.8 / -10	0.17	0.21	0.13	0.15
-1.2 / -15	0.15	0.52	0.12	0.38

Bode-type frequency distribution plots (Figure 2-D and 2-E) reveal useful information especially on the fuel electrode: an evident peak at low frequencies (1 Hz) related to gas conversion processes decreases and slightly shifts to higher frequencies with the increase of current density. At -1.2 A/cm^2 the peak rises again, indicating a gas conversion limitation. With this configuration, a second smaller peak at 60 Hz is also visible, especially at lower temperature. Current increase also reveals a minor peak at high frequencies (10 kHz) linked to the charge transfer process. On the whole, temperature variation only affects peak magnitude and not the related frequency at different current values.

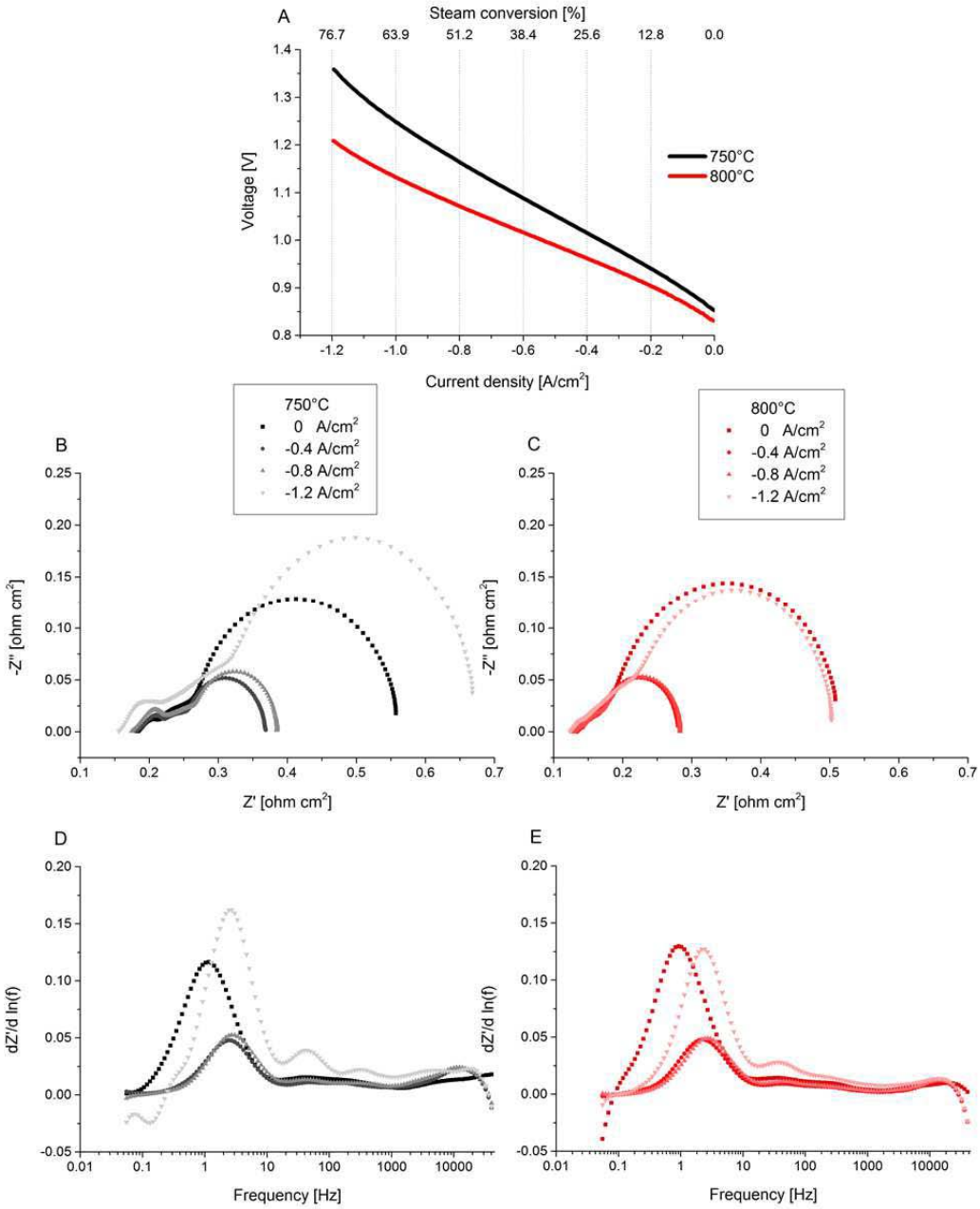

Figure 2. A: I-V curves plot at 750°C and 800°C (90% H_2O – 10% H_2 inlet molar fractions). B, C: Nyquist plot at different current density (0, -0.4, -0.8 and -1.2 A/cm^2), respectively 750°C and 800°C. C, D: real part of impedance derivative over frequency logarithm derivative plot for different current density (0, -0.4, -0.8 and -1.2 A/cm^2), respectively at 750°C and 800°C. Z''-Z' plots have aspect scale higher than 1:1 for better visibility.

A second comparison concerns the inlet feed flow variation (100, 125, 150, 175, 200 Nml/min – 90% H_2O - 10% H_2), keeping constant the steam utilization factor at 50% during the electrochemical impedance spectroscopy measurements. In order to maintain this conversion, the current density was adjusted according to Faraday's law [4], given in Table 2. Voltage increases in a similar way according to the rise of current. Figure 3-A shows a similar trend on the I-V curves, with the one related to 100 Nml/min that obviously exhibits an earlier concentration limitation above -0.8 A/cm^2.

TABLE 2. Steam electrolysis inlet feed flow variation at 50% steam conversion

Feed flow (Nml/min)	Current applied (A/cm^2 - A)	Voltage measured (V)
100	-0.52 / -6.50	1.074
125	-0.65 / -8.12	1.115
150	-0.78 / -9.74	1.154
175	-0.90 / -11.37	1.184
200	-1.03 / -12.99	1.224

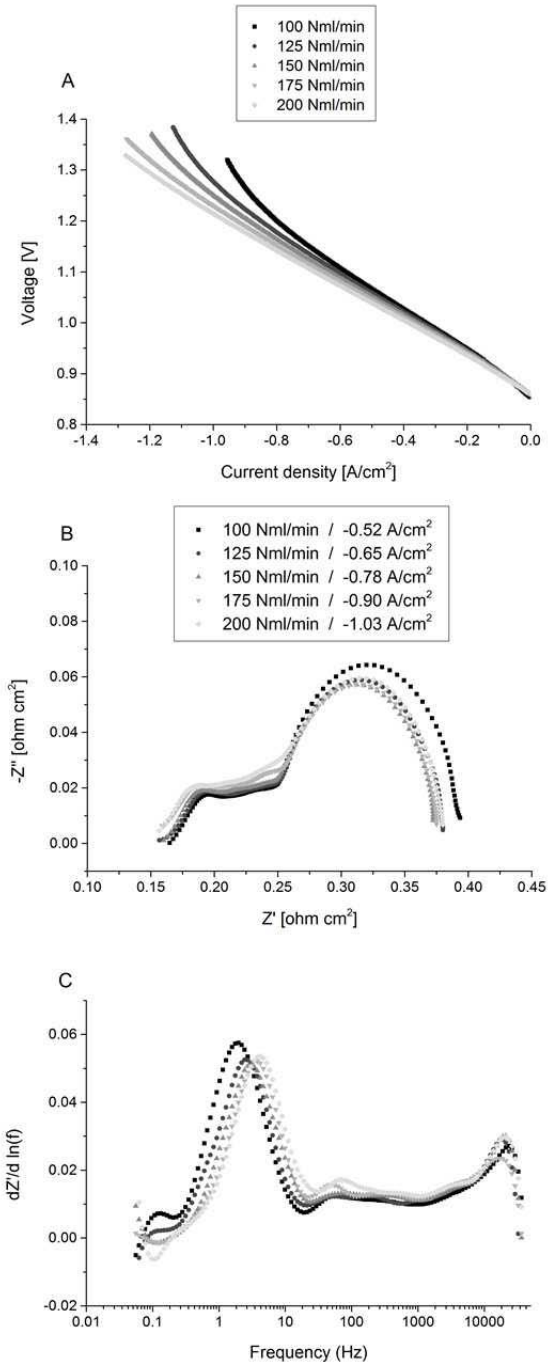

Figure 3. A: I-V curves plot at different inlet feed flow (90% H_2O – 10% H_2 inlet molar fractions). B: Nyquist plot at constant steam conversion (50%). C: real part of impedance derivative over frequency logarithm derivative plot at constant steam conversion (50%). Z''-Z' plots have aspect scale higher than 1:1 for better visibility.

Equation [5] represents the electrical conversion efficiency calculation, which essentially depends on the thermo-neutral and operating voltages (13). The first one is fixed and is determined by inlet gas composition and temperature. Therefore, the higher the operating voltage, the lower the hydrogen electrical conversion efficiency. For this reason, lower inlet feed flow guarantees better conversion efficiencies, but also a lower hydrogen outlet flow produced with the same active electrode area. In addition, thermal stability of the system depends on the operating voltage, since only a higher value compared to the thermo-neutral voltage allows positive net heat production of the system (ohmic losses greater than the heat required by endothermic electrolysis reaction). In this regard, the inlet feed flow can also be chosen according to the voltage required.

$$\eta_{conversion} = \frac{\Delta H_R \dot{N}_{H_2}}{P_{el}} = \frac{\Delta H_R}{2 F V_{op}} = \frac{V_{tn}}{V_{op}} \quad [5]$$

Nyquist plot (Figure 3-B) indicates a slight increase in ohmic resistance lowering the inlet flow, while the polarization resistance remains mainly unaffected. This effect can be explained with the small increase in temperature due to greater current densities applied to keep constant the conversion factor. Figure 3-C displays a shift to higher frequency with the rise of feed flow, which could represent a change in the gas diffusion process.

In general, the five conditions analyzed with EIS show a similar behavior, indicating that the system response to a frequency variation depends on the local processes occurring inside the cell, rather than on the specific value of current or feed flow. OCV values are slightly larger at higher inlet feed flow.

In addition, air flow variation was examined, but results did not show clear effects on performances and impedance response, therefore these data are not reported here.

Co-electrolysis

In the co-electrolysis mode steam/carbon dioxide molar fractions were varied, keeping constant feed flow (150 Nml/min – 10% H_2) and air flow (500 Nml/min). In order to prevent possible degradation, maximum voltage of 1.5 V and maximum current density of -1.2 A/cm^2 (15A) were set as limiting conditions. Steam electrolysis data (90% H_2O - 10% H_2) are reported for comparison. A different load (0.4 kg/cm^2) was applied on this cell with respect to the electrolysis experiment reported above. In this case performances are inferior due to poorer contact (higher ohmic resistance of 0.02 ohm×cm^2).

Figures 4-A and 4-B display I-V curves at 750°C and 800°C. Unlike the previous sensitivity analyses, both the increasing and decreasing phases during the potentiostatic measurements are reported in these plots, since an unusual hysteresis trend is manifest (more evident at 800°C). A slight hysteresis with steam electrolysis is always noticeable after an I-V acquiring procedure, since the temperature during the decreasing phase is higher and thus slightly improves the overall performance (in the plot the decreasing phase lies below the increasing phase). In this case, however, the direction of the hysteresis is opposite (worse performance on the return scan) and the shift between the forward and backward curves is more pronounced. This phenomenon is evident at high inlet CO_2 concentration (> 45%) and for current densities larger than -0.6 A/cm^2.

Especially at 800°C, below -0.6 A/cm^2 the I-V curves trends are similar. In the case with 65% of inlet CO_2 molar fraction, the discrepancy between increasing and decreasing I-V is maximum and this could indicate a lack of equilibrium in the system. At low CO_2 molar fraction, a small mismatch between the two curves is also noticeable, but it could be caused by a temperature effect as explained previously. In general, performances are better at 800°C and OCV values slightly decrease with the CO_2 inlet molar fraction. In addition, at 800°C it is possible to notice a variation in the slope at about 1.45V, which can indicate a modification in the electrochemical reactions pathway.

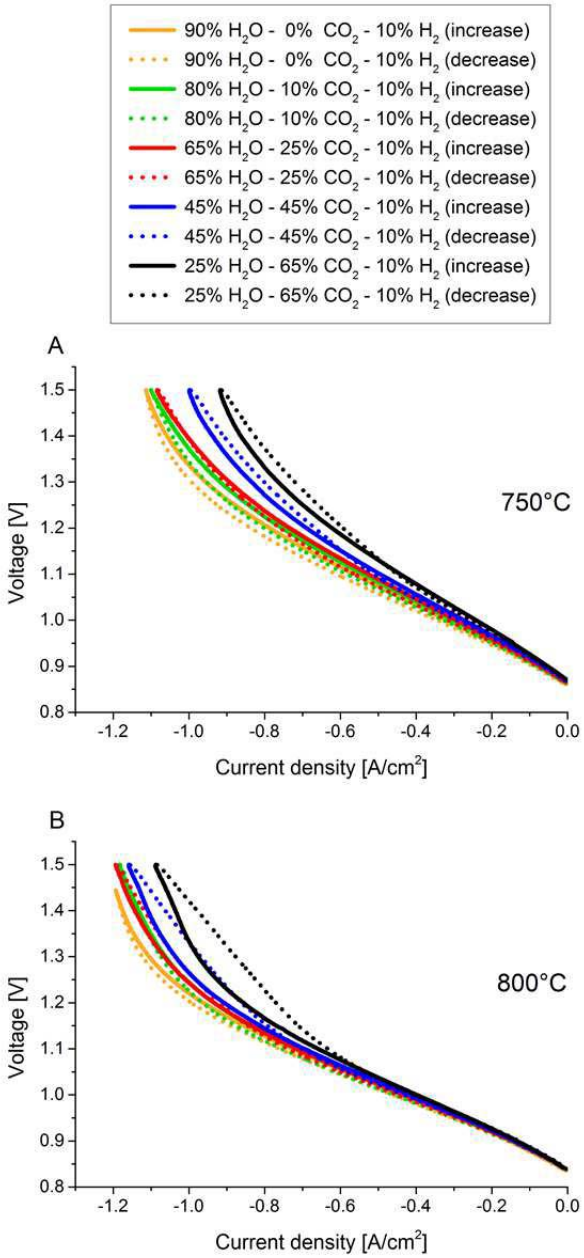

Figure 4. A, B: I-V plots of different inlet species molar fractions at 750°C and 800°C (150 Nml/min total inlet feed flow).

Figures 5-A, 5-B and 5-C represent Nyquist plots at different current density values (0, -0.4 and -0.8 A/cm^2) and constant temperature (750°C). The values of ohmic and polarization resistances obtained from the previous figures are listed in Table 3. In

general, ohmic resistance lowers with current increase, probably due to the rise of temperature. Higher values correspond to the maximum inlet CO_2 fraction (65%) and, for this reason, all the associated curves appear shifted to the right. This difference, in particular at OCV, could be related to degradation occurring at high CO_2 concentration. Further studies will be conducted in this direction. As previously shown in the steam electrolysis section, polarization resistance first decreases from 0 to -0.4 A/cm^2 and then rises again at -0.8 A/cm^2, where here it is strongly related to the CO_2 inlet fraction. Figure 5-C in particular demonstrates a considerable increase in both real and imaginary part of the impedance.

TABLE 3. Co-electrolysis ohmic and polarization resistances

Current density (A/cm^2 - A)	**Concentration (%H_2O - %CO_2 - % H_2)**	**R_{ohm} (ohm cm^2)**	**R_{pol} (ohm cm^2)**
0	90 – 0 – 10	0.20	0.36
	80 – 10 – 10	0.21	0.36
	65 – 25 – 10	0.20	0.37
	45 – 45 – 10	0.20	0.40
	65 – 25 – 10	0.23	0.42
-0.4 / -5	90 – 0 – 10	0.20	0.21
	80 – 10 – 10	0.21	0.21
	65 – 25 – 10	0.20	0.23
	45 – 45 – 10	0.20	0.26
	65 – 25 – 10	0.23	0.28
-0.8 / -10	90 – 0 – 10	0.18	0.31
	80 – 10 – 10	0.19	0.34
	65 – 25 – 10	0.18	0.42
	45 – 45 – 10	0.19	0.54
	65 – 25 – 10	0.21	0.74

Figures 5-D, 5-E and 5-F display the derivatives of the real part of impedance over the logarithm of frequency, as previously explained. At OCV condition, the different fuel concentrations show a very similar trend and, likewise to the steam electrolysis case, a significant peak is evident at 1 Hz. At this frequency, it is possible to recognize a small increase due to the change in fuel composition, such as at 11 Hz and 1 kHz. At -0.4 A/cm^2 the peak magnitude decreases compared to the OCV condition and progressively shifts to lower frequencies (except for steam electrolysis that increases at 3 Hz). This separation of the different peaks could indicate that each mixture composition has a proper frequency related to gas conversion processes. Moreover, the peak magnitude associated to 80% H_2O – 10 % CO_2 is slightly lower compared to steam electrolysis. Similar conclusions can be inferred also at -0.8 A/ cm^2, where a conversion limit of the system is manifest, especially at high inlet CO_2 concentrations. In addition, a second peak at 2-3 kHz progressively rises at -0.4 A/cm^2, probably involving the steam consumption or CO production. At -0.8 A/ cm^2 the derivative also shifts to lower frequencies, which could indicate a charge transfer limitation at the Ni-YSZ interface and a possible change in the CO_2 reduction pathway. Besides, variation in current density not only impacts directly on the species concentration because of steam electrolysis and CO_2 reduction, but also on the reverse water-gas-shift reaction rate, which is also influenced by temperature increase.

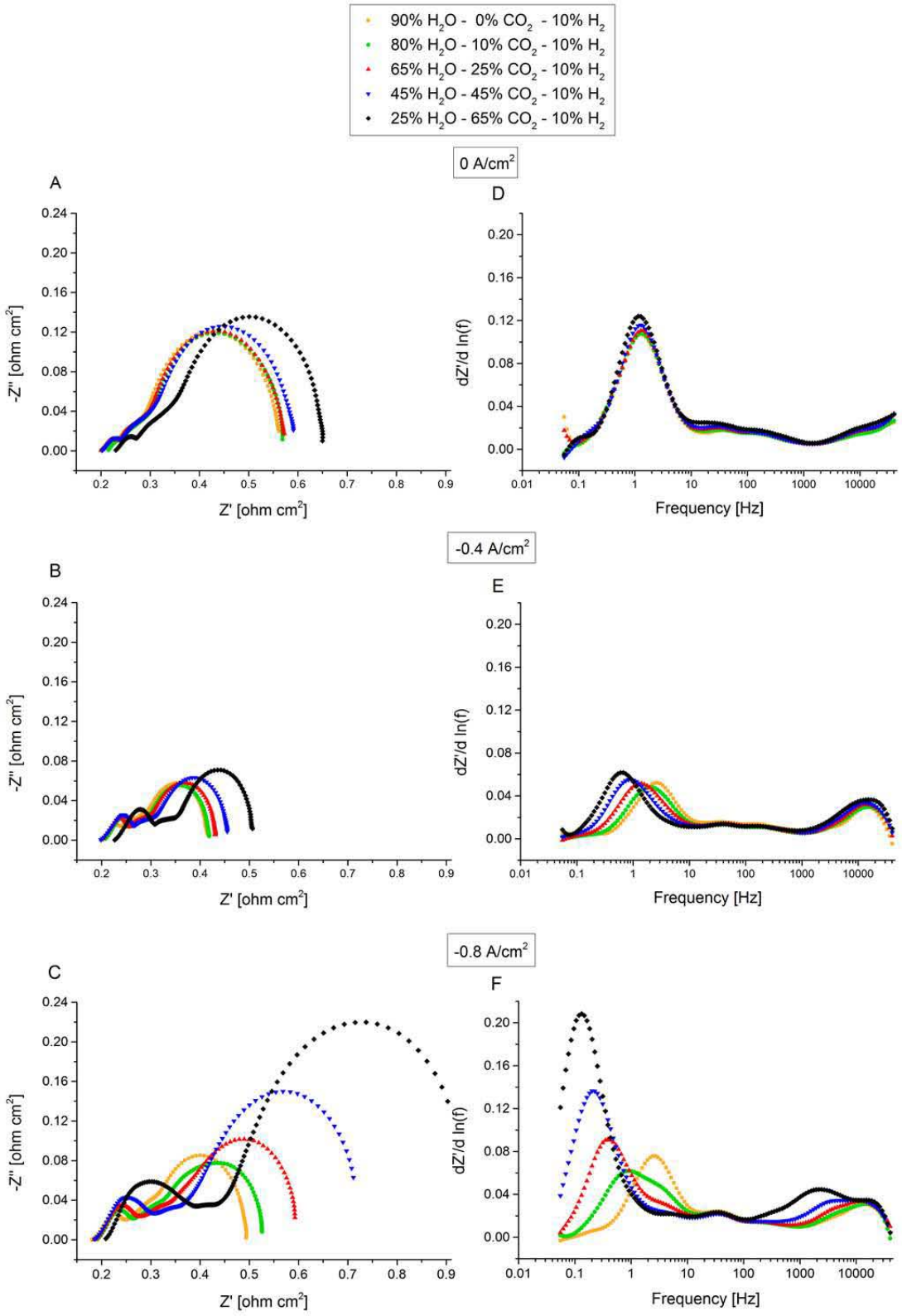

Figure 5. A, B, C: Nyquist plots of different inlet species molar fraction at 0 A/cm^2, -0.4 A/cm^2 and -0.8 A/cm^2. D, E, F: real part of impedance derivative over frequency logarithm derivative plots at 0 A/cm^2, -0.4 A/cm^2 and -0.8 A/cm^2. Z''-Z' plots have aspect scale higher than 1:1 for better visibility.

Conclusion

Steam electrolysis and co-electrolysis experiments were investigated based on differences in I-V curves and impedance spectra due to a change of operating parameters. Temperature variation during electrolysis has confirmed the strong relation between performance and temperature increase. The difference in the derivative with respect to frequency logarithm of the real part of the impedance clearly outlines a gas conversion process at 1-2 Hz that depends on the steam/CO_2 feed.

Inlet feed flow variation I-V curves highlight different ranges of operation, which can be chosen according to the hydrogen flow that has to be produced and the thermal management of the system (depending on the operating voltage). EIS measurements show similar behavior at constant steam conversion factor (and different current imposed), with a small translation of the curves toward lower frequencies at lower inlet feed flows.

In co-electrolysis mode, I-V curves demonstrate a progressive decrease in performance with the increase in CO_2 inlet concentration. Higher temperature involves also an increase in the 'inversed' hysteresis trend that appears when voltage is decreased during potentiostatic measurements. This phenomenon indicates a global non-equilibrium between the three chemical processes (steam electrolysis, CO_2 reduction and RWGS) which are strongly related and affected by current. Impedance spectra analysis seems to corroborate this hypothesis: in particular, with the increase of current density, each different inlet molar fraction in the dZ'/d ln(f) plot corresponds to a change in frequency (in the range from 0.2 to 3 Hz). At -0.4 and -0.8 A/cm^2 a significant variation in peak magnitude and frequency at 2-3 kHz was recognized, corresponding to a possible change in the CO_2 reduction pathway.

Very high inlet CO_2 molar fractions have been analyzed in order to better understand the phenomena occurring, but only steam-to-CO_2 ratios larger than 2:1 can be considered for syngas or liquid fuel (methanol) production. Degradation under such conditions was observed during the experiments and will be treated in future work.

Acknowledgements

This research was financially supported by the Swiss EOS Holding funding scheme. Cells were provided by SOLIDpower (Italy) and the evaporator was obtained from Fiaxell (Switzerland).

References

1. Q. Fu, *Syngas: Production, applications and environmental impact*, **8**, 209-240 (2013).
2. Q. Fu, C. Mabilat, M. Zahid, A. Brisse, L. Gautier, *Energy & Environmental Science,* **3 (10)**, 1365-1608 (2010).
3. S. Kim, H. Kim, K. Yoon, J. Lee, B. Kim, W. Choi, J. Lee, J. Hong, *J. Power Sources,* **280**, 630-639 (2015).

4. C. Graves, S. Ebbesen, M. Mogensen, K. Lackner, *Renewable and Sustainable Energy Rev*, **15**, 1–23 (2011).
5. http://www.solidpower.com/en/home/
6. http://www.htceramix.ch/upload/ASC-700_ASC-800.pdf
7. H. Madi, A. Lanzini, S. Diethelm, D. Papurello, J. Van herle, M. Lualdi J. Larsen, M. Santarelli, *J. Power Sources,* **279**, 460-471 (2015).
8. http://www.fiaxell.com/
9. B. Liu, H. Muroyama, T. Matsui, K. Tomida, T. Kabata, K. Eguchia, *J. Electrochem. Soc.*, **157 (12)**, B1858-B1864 (2010).
10. S. Jensen, A. Hauch, P. Hendriksen, M. Mogensen, N. Bonanos, T. Jacobsen, *J. Electrochem. Soc.*, **154 (12)**, B1325-B1330 (2007).
11. R. Barfod, M. Mogensen, T. Klemenso, A. Hagen, Y. Liu, P. Hendriksen, *J. Electrochem. Soc*., **154**, B371 (2007).
12. C. Graves, S. Ebbesen, M. Mogensen, *Solid State Ionics*, **192**, 398–403 (2011).
13. J. O'Brien, **IMECE 2008**, 68880 (2008).